JOURNAL OF SOLID STATE CHEMISTRY 112, 161–169 (1994)

Structural Aspects of Li-Doped Tubular Bismuth Cuprates ($Bi_2Sr_3Cu_{2-x}Li_xO_y$): An Electron Microscopy Study

G. Van Tendeloo,[1] B. Domengès, M. T. Caldes,[2] M. Hervieu, and B. Raveau

Laboratoire de Cristallographie et Sciences des Matériaux, Boulevard du Maréchal Juin, 14050 Caen Cedex, France

Received June 14, 1993; accepted November 5, 1993

Different new monoclinic structures have been discovered and structurally analyzed in Li-doped $(Bi_{2+}Sr_{2-x}CuO_{6+\delta})_n(Sr_{8-y}Cu_6O_{16+z})$. The new structures can be interpreted as one-dimensional nonconservative, long-period superstructures of the (unmodulated) 2201 superconducting phase. High-resolution electron microscopy and selected area electron diffraction allow the proposal of detailed models for the perfect structures with $n = 13/2$ and 15/2 as well as for the numerous structural defects.

1. INTRODUCTION

The discovery of superconductivity in the Bi–Sr–Ca–Cu–O family of materials [1–3] has stimulated chemical and structural research in related compounds. This has led to the discovery and analysis of a number of related structures. Although not all of them are superconducting, they have undoubtedly led to a better understanding of the structural properties and requirements for superconductivity. One such family with complex but fascinating structural features is the family of tubular bismuth cuprates with the general formula $(Bi_{2+x}Sr_{2-x}CuO_{6+\delta})_n(Sr_{8-y}Cu_6O_{16+z})$, with values of n varying between 4 and 7 (4–8). Its structure is closely related to that of the "2201" superconducting phase; it can be described as an intergrowth along the b axis of n 2201 slices and a perovskite-related slice (4, 5). The overall symmetry of the different members of the family is orthorhombic, but several planar defects and even isolated monoclinic regions were detected by electron microscopy (7, 8). The idea of replacing some of the Cu by Li was an attempt to introduce structural changes into the structure and to (maybe) stabilize some of the higher members, or monoclinic variants of the family. These monoclinic phases were found occasionally and over very small areas in the undoped Bi–Sr–Cu–O material (9).

2. EXPERIMENTAL

Cuprates with nominal composition $Bi_2Sr_{2.9}Cu_{1.6}Li_{0.4}O_x$ were synthesized from adequate mixtures of Bi_2O_3, $SrCO_3$, CuO, and Li_2CO_3 heated in air for 12 hr at 800°C (4–6). The obtained powder was reground, pressed into pellets, and heated in air another 12 hr at 800°C; this procedure was repeated several times.

Electron microscopy observations were performed at 200 kV using a Jeol 200CX side-entry microscope with ±60° tilting possibilities to explore reciprocal space and using a Topcon 002B microscope with a point resolution of 0.18 nm for high-resolution observations.

3. STRUCTURE OF THE TUBULAR PHASES

Structural details of the orthorhombic phases can be found in (4, 5); we will repeat here only the basic features necessary to understand the present observations. In Fig. 1 we have represented one member of the family together with the (unmodulated) structure of the basic 2201 phase (Fig. 1a) viewed along the perovskite [110] direction. The value of n ($n = 4$ in the case of Fig. 1b) equals the number of copper polyhedra along the b axis. Along the c axis of the orthorhombic structure, slabs of the 2201 structure (indicated by S in Fig. 1b), being four copper polyhedra wide along b, are stacked and are interrupted by a layer of perovskite material (indicated by P in Fig. 1b). As a result the c axis is approximately equal to the c axis of the 2201 structure and does not change dramatically with n ($c = 2.397$ nm for $n = 4$; $c = 2.437$ nm for $n = 7$) (6). Also the a-axis ($a = 0.54$ nm) remains more or less constant for different n values. Within this structure considerable strain or misfits must be associated with the tunnel positions indicated by stars in Fig. 1b. Here the oxygen positions are supposed to be highly disordered between two positions along the a axis (6). It is very much expected that these sites are only partially occupied.

[1] On leave from EMAT, University of Antwerp (RUCA), Groenenborgerlaan 171, B-2020 Antwerp, Belgium.

[2] On leave from Instituto de Ciencias de Materiales CSIC, Campus UAB, 08193 Bellaterra, Spain.

0022-4596/94 $6.00

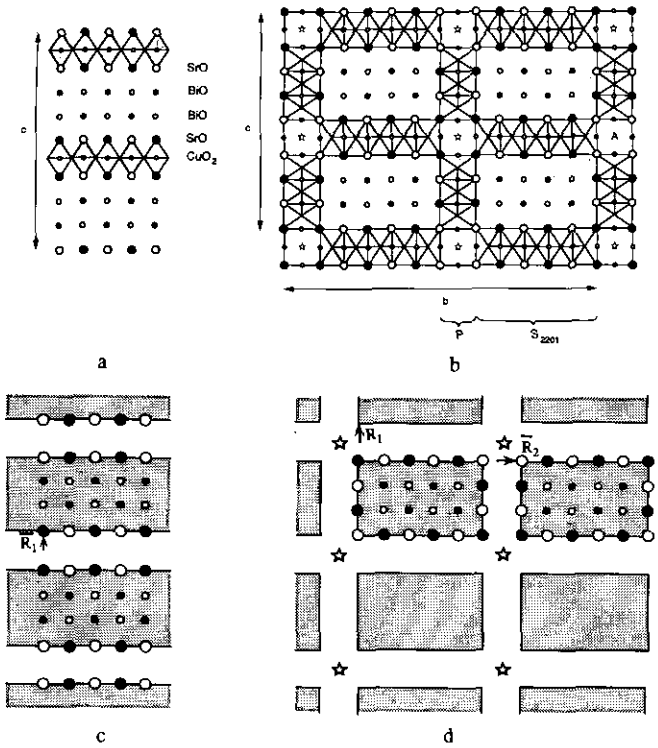

FIG. 1. Structural representation projected along the [100] direction of (a) the 2201 basic structure, and (b) the orthorhombic tubular $n = 4$ structure of the BiSrCuO phase. Schematic representation of (c) the 2201 basic structure and (d) the orthorhombic tubular structure.

A model for the monoclinic phase has been proposed based on high-resolution observations. The proposed structure is directly related to the orthorhombic tubular phase by a mechanism of shifting the BiO layers (9).

3. OBSERVATIONS

3.1. Electron Diffraction Data

The vast majority of the nominally prepared $Bi_2Sr_{2.9}Cu_{1.6}Li_{0.4}O_x$ material shows monoclinic symmetry rather than the orthorhombic symmetry found in the undoped material. Electron diffraction patterns along different basic zone axes (Fig. 2) allow the deduction of the unit cell parameters as well as the space group. Figure 2a is identical to the (a^*c^*) section of the 2201 phase; the c centering is obvious from the shift of the uneven rows with respect to the even rows. In the perpendicular section of Fig. 2b it is clear that because of the long modulation along b^* the structure is no longer orthorhombic but monoclinic with an angle $\alpha = 96°$. The third section (a^*b^*) is in agreement with the previous ones and leads to the monoclinic real space unit cell description

$$a_m = 0.54\ \text{nm}$$
$$b_m = 4.60\ \text{nm}$$
$$c_m = 2.44\ \text{nm}$$
$$\alpha = 96°.$$

The choice of these monoclinic axes with the a_m^* and c_m^* axes along the a^* and c^* axes of the orthorhom-

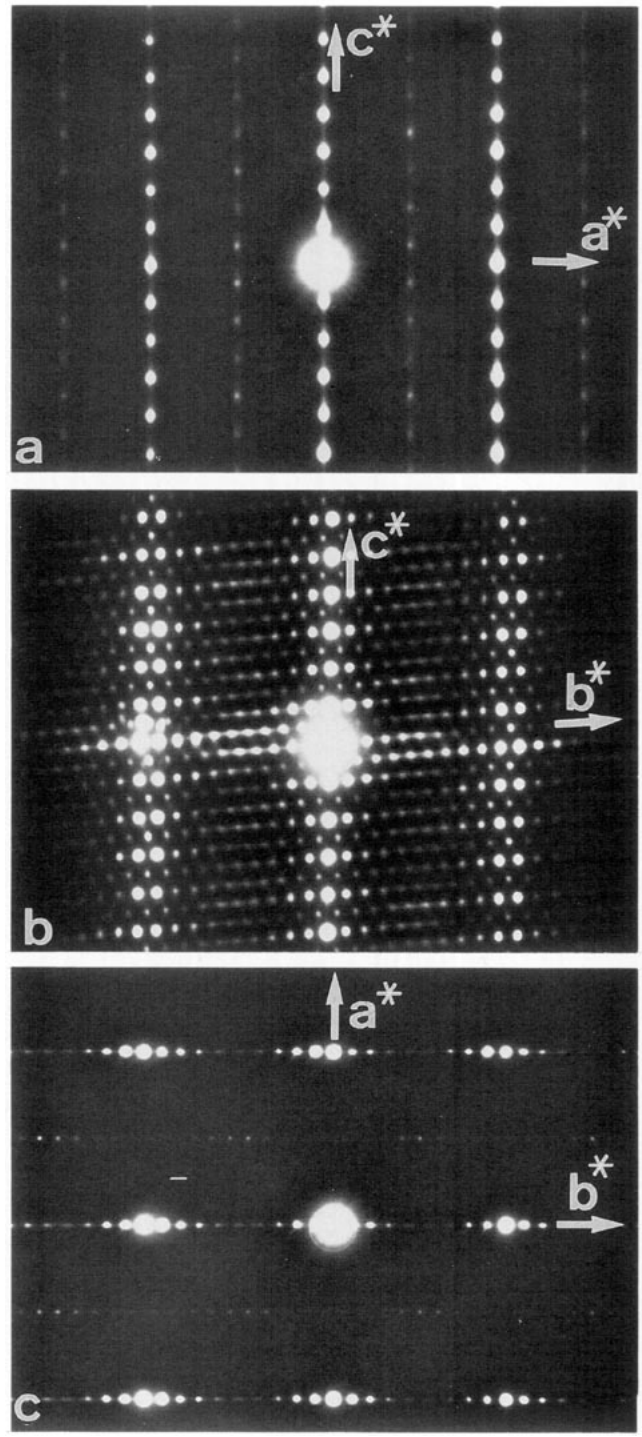

FIG. 2. Basic electron diffraction patterns of the monoclinic tubular structure: (a) a^*c^* section, (b) c^*b^* section, and (c) a^*b^* section.

bic 2201 structure and the b_m^* axis along the direction of the monoclinic modulation is useful in order to describe the structural relationship between both, but is not in agreement with the "International Tables for X-Ray Crystallography"; because of the choice of a nonprimitive cell, extinctions are not in agreement with any of the space groups. However, with a different choice of axes, the $a_{m'}^*$ axis along $[011]_m^*$, the $b_{m'}^*$ axis along a_m^*, and the $c_{m'}^*$ axis remaining along c_m^*, the extinction conditions are in agreement with the space group $C2/m$ (or $C2$ or Cm, since the latter cannot be distinguished in diffraction from the centered space group $C2/m$). Despite the International Table requirements, we will adapt throughout this text the above-mentioned nonprimitive unit cell description because of its simple structural relation with the perovskite structure as well as with the 2201 structure. Moreover the same notation has been used in previous papers on related materials (4–8).

Since the a axis remains approximately unaltered for different monoclinic structures, the most instructive section is [100]; it is shown in Figs. 3b and 3c for two different n values and compared with a corresponding pattern (Fig. 3a) for the orthorhombic tubular structure ($n = 4$). A common feature of all these patterns is the intensity distri-

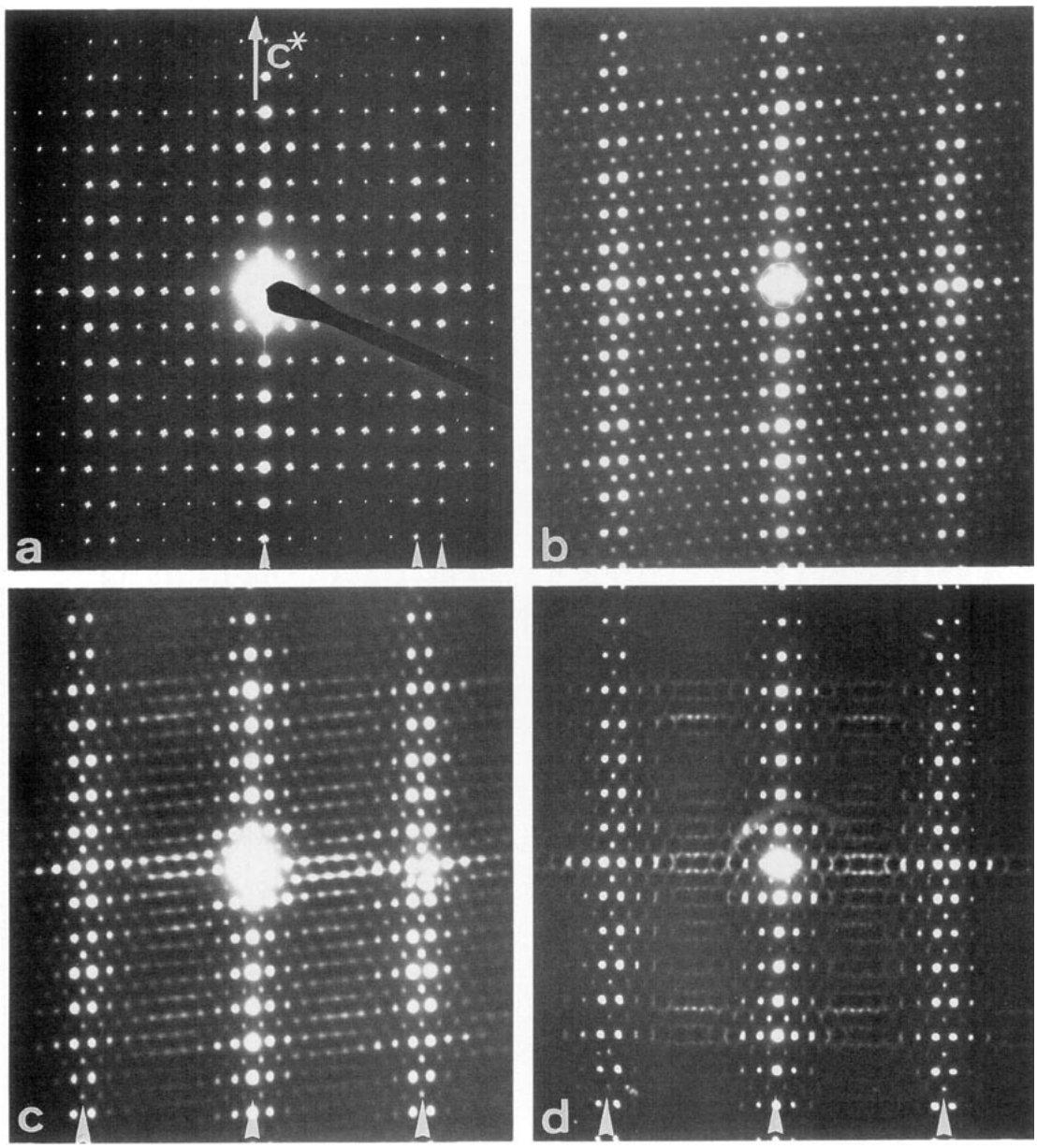

FIG. 3. Corresponding electron diffraction patterns for (a) the orthorhombic phase with $n = 4$, (b) the monoclinic phase with $n = 13/2$, (c) the monoclinic phase with $n = 15/2$, and (d) a defective monoclinic phase.

bution: parallel to the c^* axis, regions of more intense reflections occur at a distance of approximately 4.0 nm^{-1}; this effect is even more pronounced for some defect-containing structures, producing a pattern such as that in Fig. 3d. These phenomena are very common in long-period superstructures or shear structures. The present diffraction patterns can indeed be understood as being derived from the basic 2201 pattern. As indicated in the schematic representation of Fig. 1, the $n = 4$ tubular structure can be considered as strips of unmodulated 2201 (indicated S_{2201}) separated by a perovskite-type strip (indicated P). The 2201 structure itself can be considered as a stacking along the c axis of bands of four layers of the rock salt type (SrO–BiO–BiO–SrO) separated by a layer of the perovskite type (see Fig. 1). The rock salt regions (strips in the 2201 structure and rectangular islands in the tubular structure) consist of the [100] projection of a regular square arrangement of heavy ions (Sr or Bi) separated by approximately $u = 0.25$ nm (see Fig. 1d). A diffraction pattern of such an infinite square ion configuration would consist of a square lattice of reflections separated by 4.0 nm^{-1}. The perovskite strips in the 2201 structure actually introduce a shift in the c direction every 1.22 nm of $R_1 = [0\ 0\ u\sqrt{2}]$ between successive rock salt bands. The unmodulated 2201 structure is therefore a long-period modulation of the basic rock salt structure and its diffraction pattern can be deduced from the square rock salt pattern according to the rules for the long-period superstructures [10, 11], giving rise to a periodic modulation along c^* with a periodicity of 0.82 nm^{-1} and introducing a spot splitting of the basic rock salt reflections according to the value of $g \cdot R_1$. The orthorhombic tubular structure is generated from the 2201 structure by introducing a second long-period modulation along the b axis, with a displacement vector $R_2 = [0\ u\sqrt{2}\ 0]$. Alternatively it can be described as a two-dimensional modulated structure of the rock salt structure. The basic 2201 reflections will therefore also split into two satellites according to the value of $g \cdot R_2$, which in this case is approximately 1/2 for all reflections parallel to c^* and having $k = 1$. The intensity of the satellites decreases with increasing distance from the basic reflections. Therefore we observe in the experimental diffraction pattern of Fig. 3a a single intense row of $00l$ reflections ($g \cdot R_2 = 0$) and two more intense maxima for all reflections with $k = 1$ ($g \cdot R_2 \approx 1/2$). The rows are indicated by a single and a double arrowhead, respectively, in Fig. 3a.

The same diffraction features hold for the monoclinic variants of these structures; we can therefore also consider these as two-dimensional modulations of the basic rock salt structure or as one-dimensional modulations of the 2201 structure, the monoclinic angle resulting from the fact that the shear planes are (on average) no longer perpendicular. From the diffraction data only, we cannot predict further details for the atomic structure of the monoclinic tubular structures. A possible model has been put forward in (7), but as we will see from the high-resolution observations, it does not hold for the present Li-doped material.

3.2. *HREM Data*

High-resolution images have been obtained along all three reciprocal lattice sections discussed above; it is clear, however, that only the images along the [100] axis reveal the information needed to propose more detailed structural models for the monoclinic phases. Such an image is seen in Fig. 4 for a defocus value around −50 nm. Rectangular blocks of white dots, 4 rows high and several rows (between 8 and 10) wide, can be clearly discerned. As suggested from the projected crystal potential of an orthorhombic variant with $n = 4$, as well as from the calculated images in Fig. 5, these white dots are to be associated with the heavy Bi and Sr ions in the rock salt configuration as discussed before. The darker areas separating the different blocks are the perovskite regions, formed by the CuO_6 octahedra. Note, however, that in the present observations the different blocks no longer invariably have the same length.

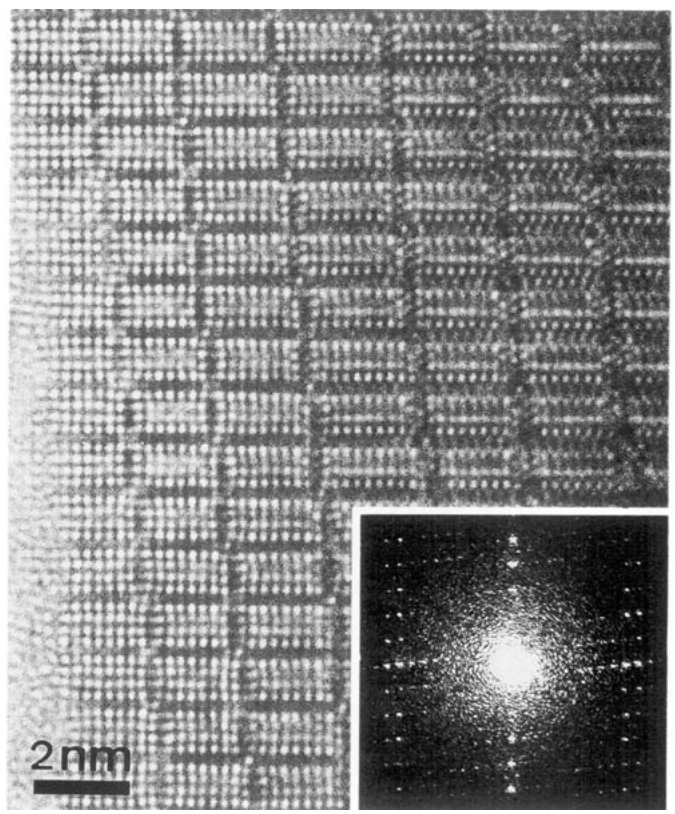

FIG. 4. High-resolution image along [100] of a periodic monoclinic tubular structure; the optical diffraction is shown as an inset.

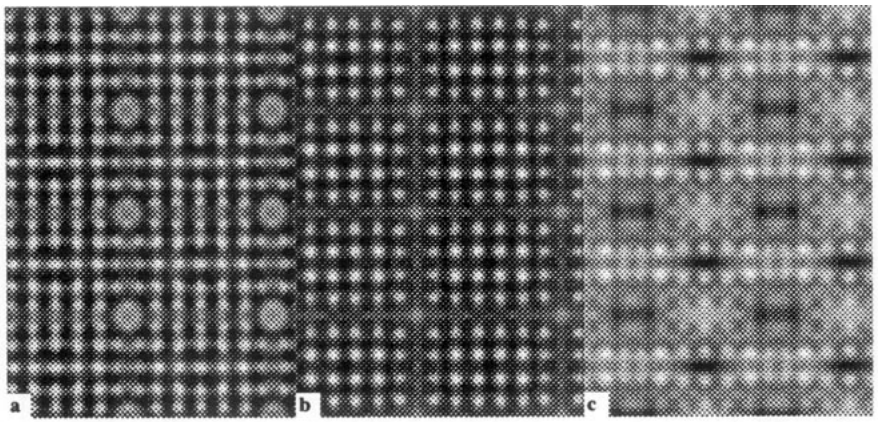

FIG. 5. Calculated HREM images for a thickness of 3.2 nm and different defocus values: (a) $\Delta f = -30$ nm, (b) $\Delta f = -50$ nm, and (c) $\Delta f = -140$ nm. For $\Delta f = -50$ nm the heavy ions (Sr and Bi) are imaged as bright dots.

When two blocks of different length, e.g., blocks of $n = 6$ (8 subunits wide) and blocks of $n = 7$ (9 subunits wide), are stacked along the c direction, one can no longer maintain the square sites and the local orthorhombic symmetry as indicated by a star in Figs. 1b and 1d. The sites become—in projection—lozenge shaped, as can be seen at different spots in Fig. 4. As a consequence the (010) shear planes form a non-90° angle with respect to the (001) planes. If such shifts occur regularly the structure becomes monoclinic. One can easily calculate that if, along the c axis, the shifts occur in every unit cell such as in Fig. 6a, the monoclinic angle is $\alpha = 100°$; this structure has actually been observed in the monoclinic 5 tubular structure (8). If the shift occurs in every other unit cell, as in Fig. 6b, the monoclinic angle α equals 96°. The latter value has actually been observed in the experimental diffraction patterns in Fig. 3. It is obvious from the HREM in Fig. 4 that there is a clear tendency to have a

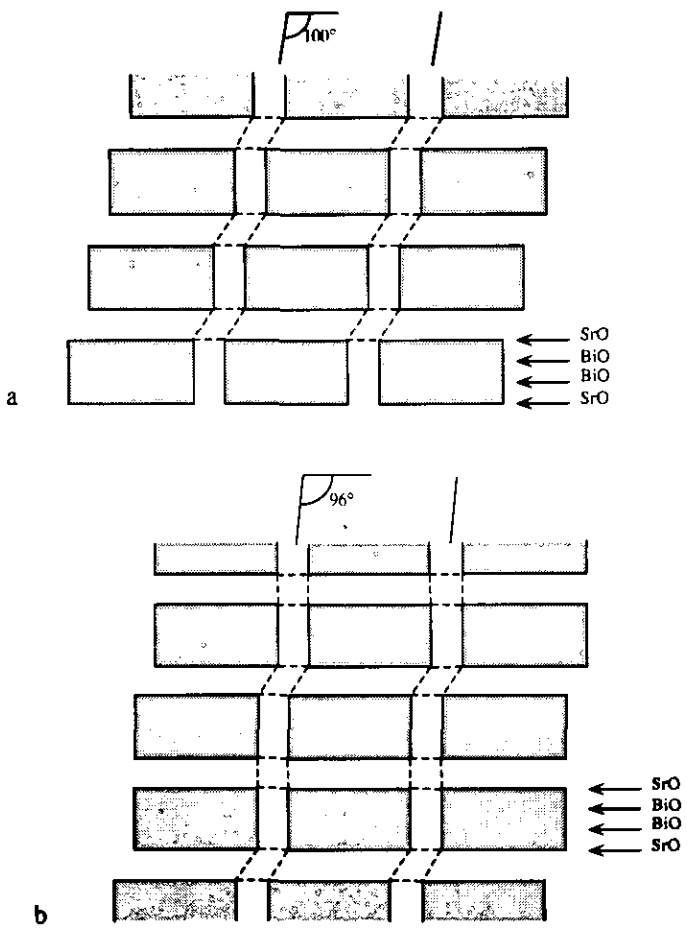

FIG. 6. Different monoclinic versions, deduced from the orthorhombic structure. (a) $\alpha = 100°$, by introducing shifts every unit cell, and (b) $\alpha = 96°$, by introducing shifts every two unit cells.

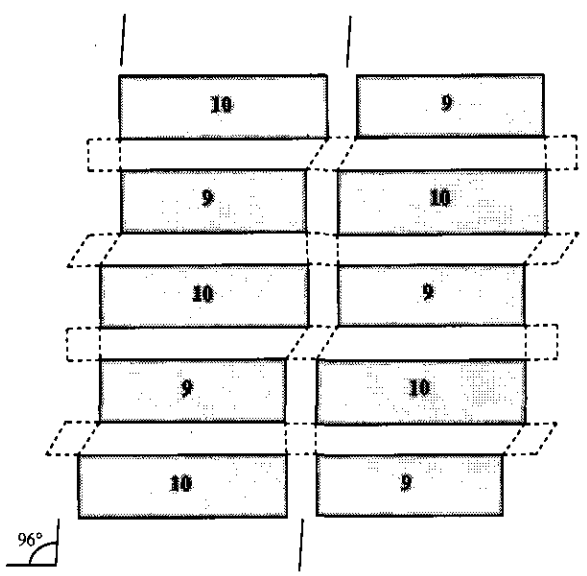

FIG. 7. Schematic representation of the monoclinic structure according to the HREM observations. The numbers correspond to the number of bright dots in the HREM images; the actual n value for this monoclinic phase is therefore $n = 15/2$.

shift in every other unit cell. Moreover the length of the blocks along the *b* axis is not constant and alternates. So the monoclinic structure corresponding to the diffraction pattern in Fig. 3c consists of a two-dimensional patchwork of blocks of different length varying along *b* as well as along *c* (see Fig. 7).

By careful analysis of the HREM images, such as that in Fig. 8, one can hope to obtain some information on the atomic configuration in the square or lozenge-shaped tubes occurring at the intersection of four perovskite blocks. The coordination of copper at the intersections is indeed still unknown. Comparing the experimental image in Fig. 8 with the calculated images in Fig. 5 reveals a number of small differences. In the latter the 4×6 blocks of bright dots are undistorted and the block is perfectly rectangular; in the experimental image the outer (010) planes (vertical in Fig. 8) are always curved, and moreover there are some weaker intensity maxima visible inside the square or lozenge-shaped tubes. Such intensity variations are not expected for the undeformed structure and do not appear in the calculated images for any value of defocus or thickness. We will further try to interpret these data in the function of structural occupancies.

As already seen from the diffraction data in Fig. 3 and from the high-resolution observations in Fig. 4 or 8, a number of structural defects can be expected:

(a) The value of *n* may deviate from the ideal sequence along the *c* direction. Such defects are seen frequently and they introduce a local change in the monoclinic angle α; i.e., a shift does not occur necessarily every two unit cells along *c* (see, e.g., Fig. 9).

(b) The value of *n* may deviate from the ideal sequence along the *b* direction (see Fig. 9). Such defects will intro-

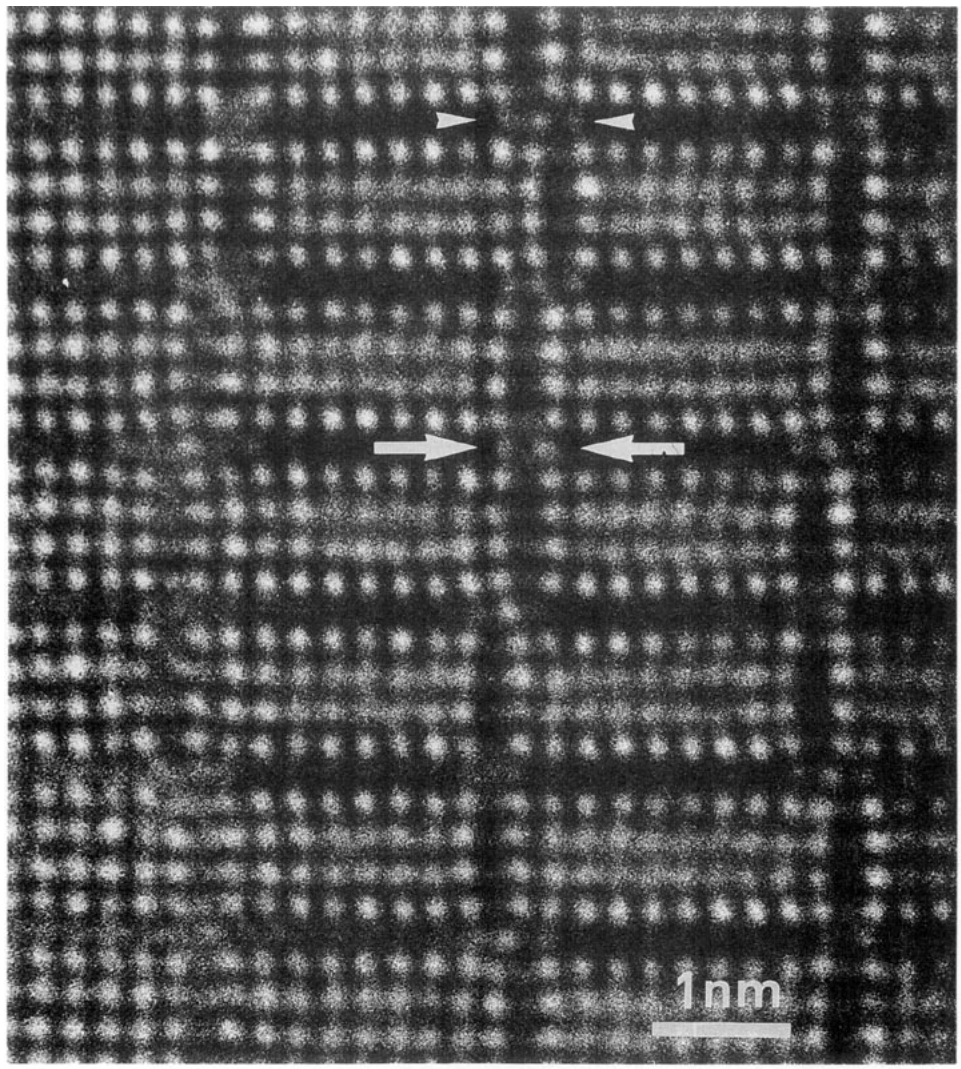

FIG. 8. High magnification of a tubular phase showing orthorhombic as well as monoclinic blocks and revealing details about the intersection of different blocks which can be rectangular (large arrows) or lozenge shaped (arrowheads).

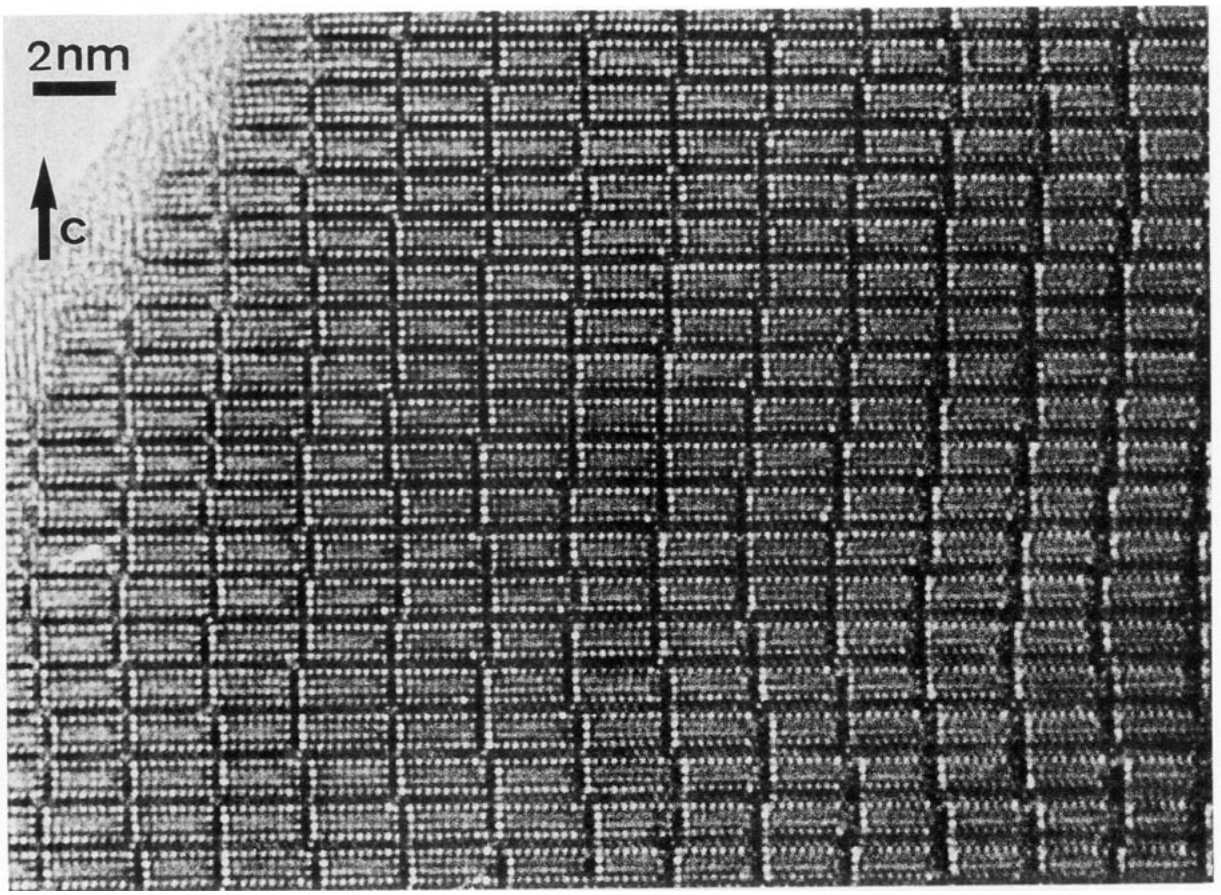

FIG. 9. HREM of a highly disordered monoclinic tubular structure showing several stacking errors.

duce a streaking along b^* in the diffraction pattern; an example is seen in Fig. 3b.

(c) Even when unfaulted, the monoclinic structure may form in two symmetry-related variants with respect to the orthorhombic structure; such a twin-type defect is seen in Fig. 10a.

(d) Superdislocations in the modulated structure have regularly been observed (Fig. 10b), and they have already been described in the orthorhombic structure (6).

4. DISCUSSION

The undistorted structure proposed here for the monoclinic phase is different from the one found by Caldes *et al.* (9) or by Matsui *et al.* (12). They both claim that the monoclinic shifts along the b axis are introduced between the $(BiO)_2$ layers; this is not illogical because the Bi superconductors all tend to cleave on the BiO planes (13, 14). However, this assumption is inconsistent with the present observations on Li-doped material. The comparison with the calculated images clearly shows that at a defocus value of -50 nm, we do image the Bi and Sr ions as bright dots. The shifts in these images (Figs. 4, 8, and 9) undoubtedly occur at the intersection of the perovskite layers. Some of these conclusions could already be drawn from the observations made for the monoclinic $n = 5$ structure (8).

It is not clear whether two different structures exist: one with a shift at the BiO layers and another with shifts at the perovskite layers. The HREM images presented in (9) do not show enough detail to decide unambiguously, while the published images in (12) are of a too low magnification to deduce important details. However, our observation and evidence are unambiguous.

The second important point is the exact atom configuration at the intersection, for the orthorhombic configuration as well as for the monoclinic configuration. For the orthorhombic tube configuration one notices in Fig. 8 a strong deformation of the Sr configuration around the tube; moreover there are in general four weaker intensity maxima at, or close to, the projected Cu(1) and Cu(4) positions (notation according to (5)). Very often, however, the intensity of these dots is not equal (see the large arrows in Fig. 8), indicating a partial and preferential occupation of these sites. It is very possible that in a single layer either one or the other position is occupied

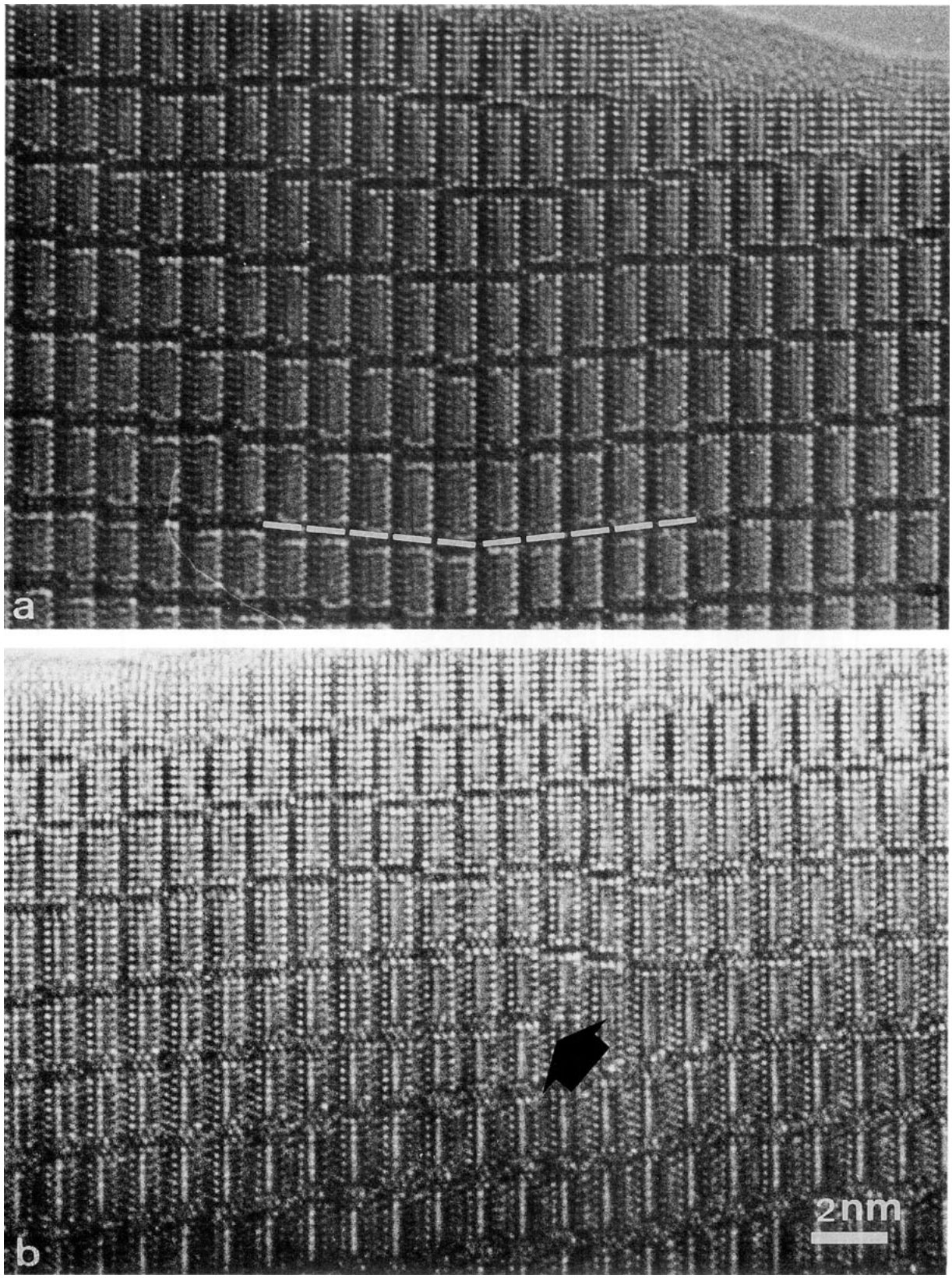

FIG. 10. HREM of defects occurring in tubular structures. (a) Twinning with respect to the (010) plane and (b) a superdislocation in the modulated structure.

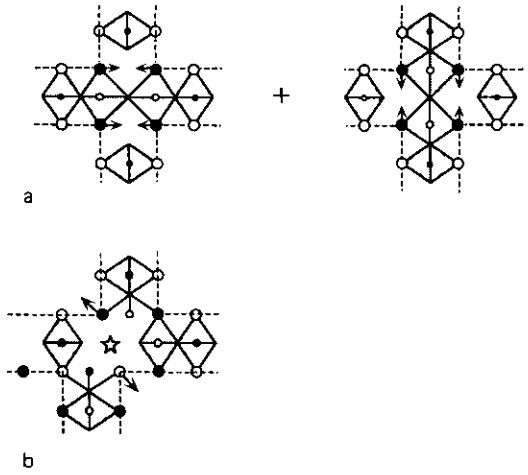

FIG. 11. Schematic structural representation of the atom configuration at (a) a rectangular intersection (as for the orthorhombic structures) and (b) a lozenge-shaped intersection (as for the monoclinic structures).

(Fig. 11a), and that along the tube axis (*a* axis) this occupation alternates. If only one Cu position out of two is occupied alternatively along the *a* axis, the octahedral coordination of copper at the intersection becomes possible, and then it is to be expected that the two distorted octahedra at the intersection will try to shear ribbons, which will pull the linking Sr ions inward, as observed in the experimental images.

The situation is different for the lozenge-shaped intersections in the monoclinic variant. Here invariably three intensity maxima are observed, with the central one being the most intense (arrowheads in Fig. 8). Moreover the Sr ions at the corners of the surrounding blocks are displaced away from the lozenge-shaped tube, as represented schematically in Fig. 11b; i.e., those along the short diagonal of the lozenge are displaced the most. The exact atom configuration and coordination, however, cannot be determined from the HREM images only.

By atomic absorption we have determined the Li content in the material; it adds up to approximately half of the nominal composition, i.e., $Li_{0.2}$. If the Li is to enter the structure it will almost certainly occupy the Cu positions and most probably enter inside the lozenge-shaped tubes where the coordination is most distorted. This would also explain why the monoclinic structures are favored in the presence of Li and no orthorhombic phases are formed as in the case of the pure material.

5. CONCLUSIONS

Different monoclinic structures can be stabilized in the Li-doped tubular phases with general formula $(Bi_{2+x}Sr_{2-x}CuO_{6+\delta})_n(Sr_{8-y}Cu_6O_{16+z})$. Based on convincing HREM arguments, we have proposed here a structural model different from previous ones (9, 12). According to our model, any structure—orthorhombic, monoclinic, or mixed—consists of a stack of rectangular blocks, which at their intersection can be stacked vertically forming an orthorhombic variant, or shifted over one unit, creating a monoclinic variant.

REFERENCES

1. C. Michel, M. Hervieu, M. M. Borel, A. Grandin, F. Deslandes, J. Provost, and B. Raveau, *Z. Phys. B* **68,** 421 (1987).
2. H. Maeda, Y. Tanaka, M. Fukitoki, and T. Asano, *Jpn. J. Appl. Phys.* **27,** L209 (1988).
3. H. W. Zandbergen, Y. K. Huang, M. J. V. Menken, J. N. Li, K. Kadowaki, A. A. Menovsky, G. Van Tendeloo, and S. Amelinckx, *Nature* **322,** 620 (1988).
4. A. Fuertes, C. Miravitlles, J. Gonzales-Calbet, M. Vallet-Regi, X. Obradors, and J. Rodriguez-Carjaval, *Physica C* **157,** 525 (1989).
5. M. T. Caldes, J. M. Navarro, F. Perez, M. Carrera, J. Fontcuberta, N. Casan-Pastor, C. Miravitlles, X. Obradors, J. Rodriguez-Carvajal, J. M. Gonzalez-Calbet, M. Vallet-Regi, A. Garcia, and A. Fuertes, *Chem. Mater.* **3,** 844 (1991).
6. M. T. Caldes, M. Hervieu, A. Fuertes, and B. Raveau, *J. Solid State Chem.* **97,** 48 (1992).
7. M. T. Caldes, M. Hervieu, A. Fuertes, and B. Raveau, *J. Solid State Chem.* **98,** 301 (1992).
8. B. Domengès, M. T. Caldes, M. Hervieu, A. Fuertes, and B. Raveau, *Microsc. Microanal. Microstruct.* **3,** 415 (1992).
9. M. T. Caldes, M. Hervieu, A. Fuertes, and B. Raveau, *J. Solid State Chem.* **98,** 48 (1992).
10. J. Van Landuyt, R. De Ridder, R. Gevers, and S. Amelinckx, *Mater. Res. Bull.* **5,** 353 (1970).
11. D. Van Dyck, D. Broddin, J. Mahy, and S. Amelinckx, *Phys. Status Solid: A* **103,** 357 (1987).
12. Y. Matsui, S. Takekawa, K. Kishio, A. Umezono, S. Nakamura, C. Tsuruta, and K. Ibe, *Mater. Trans. JIM* **3,** 595 (1990).
13. H. W. Zandbergen, P. Groen, G. Van Tendeloo, J. Van Landuyt, and S. Amelinckx, *Solid State Commun.* **66,** 397 (1988).
14. E. A. Hewat, P. Bordet, J. J. Capponi, C. Chaillout, J. L. Hodeau, and M. Marezio, *Physica C* **153–155** 619 (1988).